Surface-controlled dislocation multiplication in metal micropillars

Christopher R. Weinberger* and Wei Cai

Department of Mechanical Engineering, Stanford University, Stanford, CA 94305-4040

Edited by William D. Nix, Stanford University, Stanford, CA, and approved August 6, 2008 (received for review June 24, 2008)

Understanding the plasticity and strength of crystalline materials in terms of the dynamics of microscopic defects has been a goal of materials research in the last 70 years. The size-dependent yield stress observed in recent experiments of submicrometer metallic pillars provides a unique opportunity to test our theoretical models, allowing the predictions from defect dynamics simulations to be directly compared with mechanical strength measurements. Although depletion of dislocations from submicrometer face-centered-cubic (FCC) pillars provides a plausible explanation of the observed size-effect, we predict multiplication of dislocations in body-centered-cubic (BCC) pillars through a series of molecular dynamics and dislocation dynamics simulations. Under the combined effects from the image stress and dislocation core structure, a dislocation nucleated from the surface of a BCC pillar generates one or more dislocations moving in the opposite direction before it exits from the surface. The process is repeatable so that a single nucleation event is able to produce a much larger amount of plastic deformation than that in FCC pillars. This self-multiplication mechanism suggests a need for a different explanation of the size dependence of yield stress in FCC and BCC pillars.

mechanical strength | plasticity

Plastic deformation of crystalline materials is mostly carried out by the motion of dislocations, which self-organize into complex structures at the micrometer scale (1–4). Hence, the yield strength of a crystal can be modified by the interaction between dislocations and other microscopic features with comparable length scales, such as the grain size in the Hall–Petch effect (5–7) or the specimen size itself in the micro tensile and compression experiments (8–12). Many models have been proposed to explain the specimen size dependence of the yield stress of these micropillars in the absence of an imposed strain gradient (13–17).

The basic idea of the widely discussed "dislocation-starvation" model is that dislocations escape easily due to the small size of the pillar, leaving it in a "dislocation-starved" state. Plastic deformation thus requires a continuous supply of fresh dislocations, such as by nucleation from the surface, which requires a high stress. Recent *in situ* observations of Ni pillars under compression support this picture (12).

The estimated critical stress required for dislocation nucleation from the surface also shows a size dependence consistent with experimental observations (14). In a competing model, the pillar is not starved of dislocations; instead, repeated motion of some dislocations around internal pinning points sustains the plastic deformation rate (16, 18, 19). The size-dependent yield stress is attributed to the dependence of the critical stress to activate these single-arm Frank–Read sources on the dislocation length, which scales with the diameter of the pillar.

The above controversy can be resolved only if we find the answer to an even more fundamental question: How does a single dislocation, once nucleated, move inside the micropillar? The starvation model assumes the dislocation would quickly escape from the pillar. The single-arm source model requires dislocation junctions to provide internal pinning points. However, how do the junctions form in the first place, given that they are unlikely to exist in an undeformed micropillar? Although it is very difficult to observe a single dislocation moving through the pillar *in situ*, here, we show that the answer to the fundamental question can be obtained from a series of computer simulations based on the atomistic and continuum models of dislocations. The answer turns out to depend on whether the micropillar is composed of a face-centered-cubic (FCC) or body-centered-cubic (BCC) crystal.

Fig. 1*A* shows the initial condition of a Molecular Dynamics simulations of a BCC Molybdenum pillar with diameter $D = 36$ nm (see *Materials and Methods*). A mixed dislocation with Burgers vector $\mathbf{b} = \frac{1}{2}[1\,1\,1]$ is introduced on the $(0\,1\,\bar{1})$ glide plane. Fig. 1 *B–F* are a sequence of simulation snapshots under the uniaxial compression of $\sigma_{zz} = -9$ GPa and at temperature $T = 300$ K. First, the dislocation quickly reorients itself along the Burgers vector and becomes a pure screw dislocation (Fig. 1*B*), making the subsequent dislocation behavior insensitive to initial orientation. This is because in BCC metals, non-screw dislocations move much faster than screw dislocations and quickly leave the pillar. Interestingly, a cusp develops on the screw dislocation as it moves forward (Fig. 1*C*). The cusp then evolves into a dislocation loop (Fig. 1*D*). As the loop grows larger (Fig. 1*E*), the two sides of the loop eventually leave the pillar, creating three dislocation lines in the pillar (Fig. 1*F*). Two of these dislocations have the same Burgers vector and move in the same direction as the original dislocation, while the third dislocation has the opposite Burgers vector and moves in the opposite direction. The same mechanism can happen again to these three dislocations, depending on the stress state and their positions. This simulation suggests that a single nucleation event in a BCC pillar can trigger dislocation activities for a prolonged period, leading to a large amount of plastic deformation. As a result, a BCC micropillar is unlikely to be in a "dislocation-starved" state. However, it remains to be shown whether or not this conclusion is applicable to microcompression experiments on pillars with much larger diameters (300 to 700 nm) and lower applied stress (1 to 2 GPa). To show that multiplication can occur at experimental stress and diameters, we must first understand the multiplication process.

Analysis of the above MD simulation reveals the following three necessary steps for the self-multiplication process. First, the higher mobility of non-screw dislocations leads to a straight screw dislocation inside the pillar. Second, the motion of the screw dislocation in the pillar is controlled by single-kink nucleation from the surface. In comparison, kink-pair nucleation controls the motion of a screw dislocation in bulk BCC metals. Third, the trajectories of the two surface nodes closely follow a $(1\,\bar{2}\,1)$ plane and a $(\bar{2}\,1\,1)$ plane, respectively, as shown in Fig. 1*G*. There are three $\{1\,1\,0\}$ planes and three $\{1\,1\,2\}$ planes intersecting the screw dislocation line and dislocation motion on

Author contributions: C.R.W. and W.C. designed research, performed research, and wrote the paper.

The authors declare no conflict of interest.

This article is a PNAS Direct Submission.

*To whom correspondence should be addressed. E-mail: cweinber@stanford.edu.

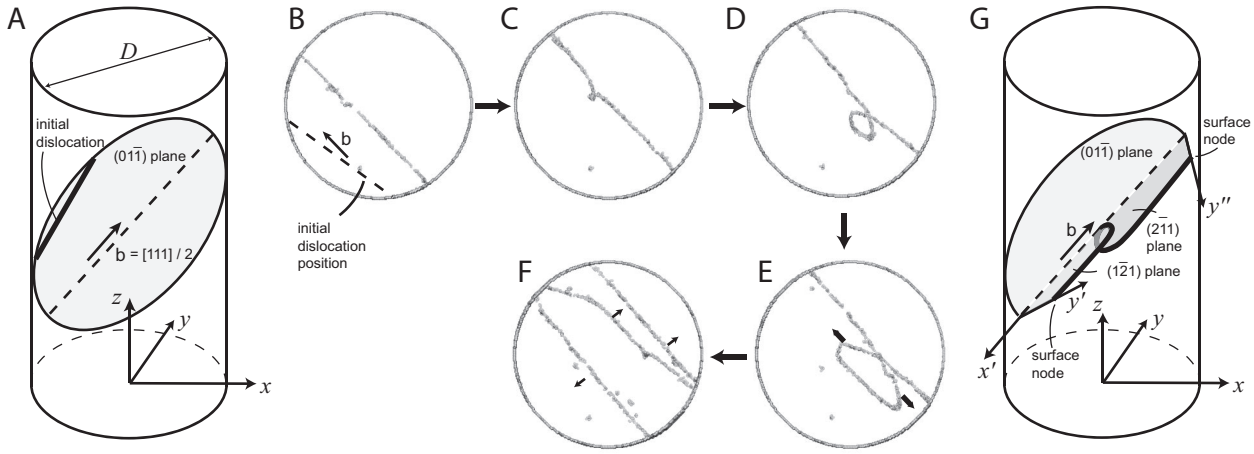

Fig. 1. The dislocation multiplication mechanism as observed in molybdenum. (*A*) Geometry of initial condition of MD simulation of dislocation motion. A mixed-dislocation with Burgers vector $\mathbf{b} = \frac{1}{2}[1\ 1\ 1]$ is introduced on the $(0\ 1\ \bar{1})$ glide plane. (*B–F*) Snapshot of MD simulation (top view). Only atoms whose central symmetry parameter (21) are sufficiently different from that of a perfect crystal are plotted, showing the dislocation core and cylinder surface. The arrows in *E* and *F* indicate the direction of dislocation motion. (*G*) Schematics of the 3D geometry of the dislocation line in *E*, which contains a loop.

both {1 1 0} and {1 1 2} planes has been observed in bulk BCC metals. In our simulations, the plane on which a surface node moves depends on stress, temperature and the empirical potential model. However, in all of our compression simulations that cover a wide range of conditions, the two surface nodes always choose to move on two different planes. Therefore, the two surface nodes are nucleation sites for kinks on two different planes. As these kinks move away from the surface, they eventually meet inside the pillar and form a cusp (where the line orientation changes abruptly). Further forward motion of the two surface nodes turns the cusp into a loop and transforms the original dislocation into three dislocations, similar to a Frank–Read mechanism.

Why do the two surface nodes move on two different planes? It is natural to expect that this is caused by the difference in the driving force on the dislocation line, which is proportional to the local stress, near the two surface nodes. This difference must come from the self-stress of the dislocation since the applied stress field is uniform. To test this hypothesis, we compute the Peach–Koehler force on the dislocation due to its own stress field in an elastic cylinder, using the dislocation dynamics model (see *Materials and Methods*). For simplicity, we consider a straight screw dislocation that goes through the center of the cylinder, as shown in Fig. 2*A*. Because a straight screw dislocation in an infinite isotropic elastic medium exerts no force on itself, only the image stress of the cylinder surface produces a force on the dislocation. This image force, plotted in Fig. 2*B*, is contained within the vertical $(1\ \bar{1}\ 0)$ plane and is antisymmetric along the dislocation line, pointing upward near one surface node and downward near the other. The direction of the image force is consistent with the choices of the slip planes of the two surface nodes shown in Fig. 1*G*. The opposite direction of the image force at two surface nodes also has a simple interpretation: The dislocation line can reduce its elastic energy by reducing its length, which requires it to rotate away from the [1 1 1] orientation. Therefore, the self-multiplication mechanism in BCC metal pillars has a simple geometric origin. It is interesting to note that non-planar motion of screw dislocations is known to cause debris formation in bulk BCC metals (20). Here, we show that the image stress, which is generally believed to accelerate dislocation's escape, amplifies this effect, promotes dislocation multiplication, and hence prolongs the dislocation's stay inside BCC pillars.

The same geometric effect also exists in FCC pillars, that is, a screw dislocation with a Burgers vector $\mathbf{b} = \frac{1}{2}[0\ 1\ 1]$ passing through the origin has image forces out of the $(1\ \bar{1}\ 1)$ slip plane. However, our MD simulations on both gold and aluminum show that the dislocation does not self-replicate in FCC pillars, even if we

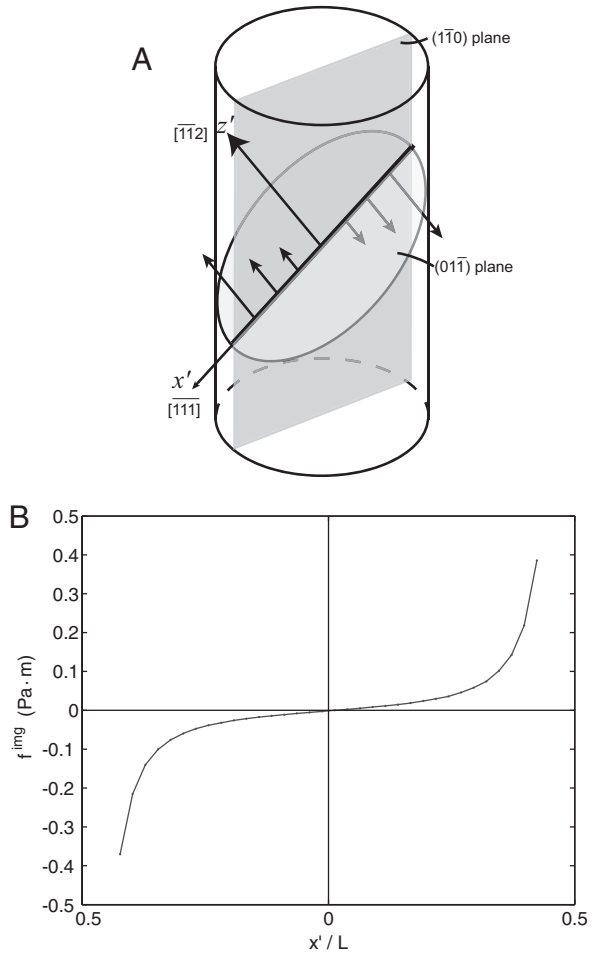

Fig. 2. The image force on a screw dislocation in the center of a pillar. (*A*) A screw dislocation passing through the center of a BCC Mo nanopillar with $D = 36$ nm. Arrows illustrate the image force due to the cylinder surface. (*B*) Image force (per unit length) along the $[\bar{1}\ 1\ 2]$ direction on the dislocation as a function of position.

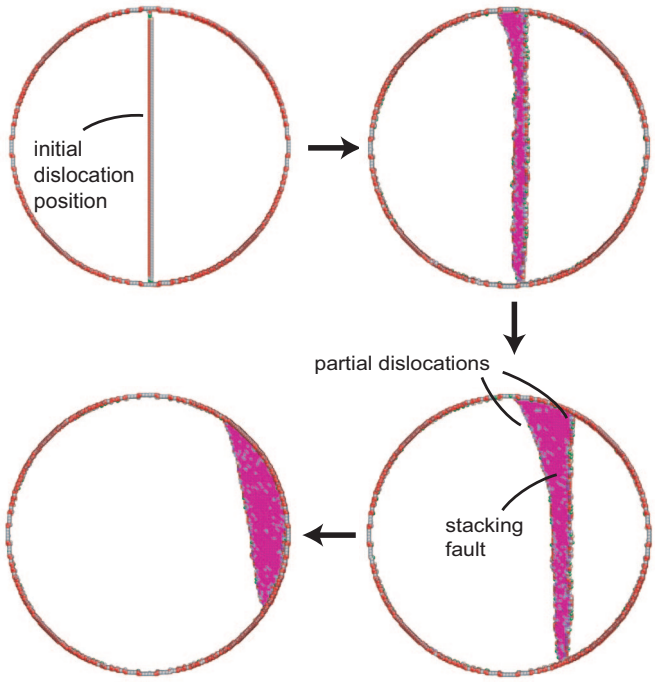

Fig. 3. Snapshots of dislocation motion in an FCC Au nanopillar of diameter $D = 36$ nm under compressive stress of 500 MPa. The asymmetric shape of the stacking fault is similar to an earlier study of dislocations in thin films (23).

initialize it to be a perfect straight screw dislocation at the center of the cylinder. As shown in Fig. 3, the main reason is the spontaneous dissociation of the dislocation on the $(1\,\bar{1}\,1)$ slip plane into two partial dislocations bounding a stacking fault. The resulting planar structure of the dislocation core confines the motion of the entire dislocation onto the same $(1\,\bar{1}\,1)$ plane. Furthermore, the dislocation mobility of screw and edge components is not very different in FCC metals. Hence, it is not very likely to find a long straight screw dislocation in FCC pillars in the first place. Dislocations in FCC metals are also highly mobile. Their motion does not require kink mechanism and is less likely to be dominated by the surface nodes. All these effects reduce the likelihood of the self-multiplication mechanism in FCC pillars. However, self-multiplication may occur in iridium, which has an exceptionally high stacking energy and a non-planar core for screw dislocations (22).

Our MD simulations also show that the dislocation behavior in BCC pillars depends on the magnitude of the compressive stress. In MD simulations starting with a straight screw dislocation at the center of the BCC pillar, a cusp always forms (we have performed MD simulation with axial stress as low as 1 GPa), but this does not always lead to multiplication. There exists a critical stress, σ_c, below which the cusp eventually drifts out of the cylinder, straightening out the dislocation without forming multiple dislocations, as shown in Fig. 4. For the Mo pillar with diameter $D = 36$ nm, the critical stress is approximately 5.5 GPa, which greatly exceeds the applied stress in the microcompression experiments (on the order of 1 GPa) (24, 25). However, our MD simulations also predict a rapid decrease of σ_c with increasing pillar diameter. In addition, the pillar diameters in the microcompression experiments (300-700 nm) are much larger than those in our MD simulations. However, it is important to know whether the critical stress σ_c for pillar diameters in experiments is lower than the observed flow stress.

To answer this question, we resort to the dislocation dynamics (DD) again. To model the dislocation behavior observed in the MD simulations, the dislocation line is divided into two sections, which are constrained on $(1\,\bar{2}\,1)$ and $(\bar{2}\,1\,1)$ planes, respectively, as shown

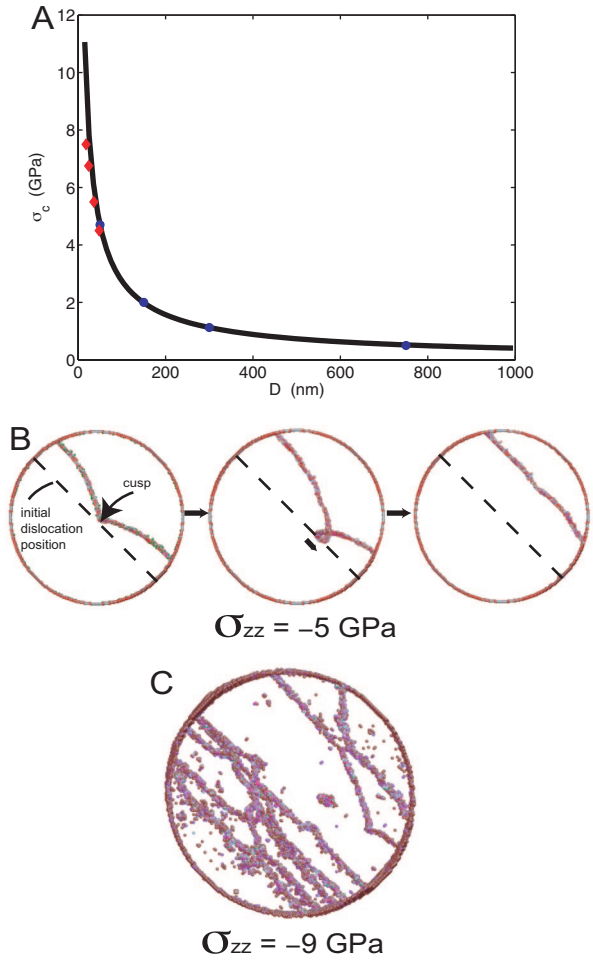

Fig. 4. The critical stress for loop formation and its effects on dislocation behavior. (*A*) Critical stress for loop formation in BCC pillar. Diamonds, MD predictions; circles, DD predictions; solid line, fitted curve $\sigma_c(D) = A/D\ ln\ D/B$ with $A = 57.5$ GPa and $B = 0.835$ nm. (*B*) Cusp escaping the pillar when applied stress is 5 GPa, lower than the critical stress. (*C*) Dislocation avalanche when the applied stress is 9 GPa, 60% higher than the critical stress.

in Fig. 1*G*. The dislocation line is discretized into straight segments connecting a set of nodes. The motion of the nodes are confined within the $x' - y'$ or $x' - y''$ plane, depending on which section they belong to (see *Materials and Methods*). Although the velocities of the two surface nodes in the y' (or y'') direction are proportional to the local Peach–Koehler force, the $y' -$ (or y'') coordinate of the interior nodes are constrained to be a fixed fraction of that of the corresponding surface node. However, the interior nodes are free to adjust their location along the x' axis. This mimics the dominance of a surface node on dislocation mobility. Interestingly, with no adjustable parameters, this simple DD model predicts a critical stress of $\sigma_c = 4.7$ GPa for $D = 48$ nm, very close to the MD observation (4.5 GPa). The DD model also clarifies the origin of the critical stress. If the applied stress is not large enough, the back stress produced by the dislocation curvature can stop the forward motion of the surface nodes before the cusp develops into a loop. When this happens, the cusp has ample time to drift away from the center and eventually escape the pillar. The critical stress at arbitrarily large diameters can now be easily predicted by the DD model (Fig. 4*A*). Both the MD and DD predictions can be fitted to a single expression similar to the well known activation stress of a Frank–Read source, $\sigma_c(D) = A/D\ ln\ D/B$, with $A = 57.5$ GPa and $B = 0.835$

nm. At experimental diameters, the predicted critical stress is well below the observed flow stress (25).

The dislocation self-multiplication mechanism in BCC pillars has the following consequences that offer an opportunity for its experimental verification, and new interpretations to some existing observations. First, through this mechanism, a single nucleation event is able to populate the micropillar with dislocations for a long time, during which another dislocation can be nucleated on a different slip system. This promotes the formation of dislocation junctions and single-arm Frank–Read sources in BCC micropillars, as postulated in some theoretical models to explain the size effect. For this reason, there should be more dislocations in a BCC pillar than an FCC pillar of the same diameter, which may be observed by transmission electron microscopy. This is consistent with the recently reported difference in the stress-strain responses of molybdenum and gold micropillars (25). Second, when the applied stress is much higher than the critical stress, both MD and DD simulations predict that each of the three dislocations created from the original dislocation can create more dislocations before they exit the pillar. It leads to an avalanche effect where a single nucleation event is sufficient to provide all the dislocations needed for a large plastic deformation at a high strain rate, as shown in Fig. 4*C*. This provides a plausible explanation for the strain-softening effect observed in recent compression experiments on BCC pillars that are initially free of surface defects (11). These pillars deform purely elastically up to 10 GPa, at which point they suddenly collapse. Third, the size-dependent critical stress for dislocation multiplication is expected to be a lower bound to the observed yield stress, because other hardening mechanisms (e.g., junction formation) can occur once the self-multiplication mechanism builds up a sufficiently high dislocation density.

In summary, we discovered a new mechanism in which a single dislocation can multiply itself repeatedly in a BCC micropillar but not in an FCC micropillar. The mechanism is the combined result of both the surface-induced image stress and surface-dominated dislocation mobility at small scales. This discovery points to the necessity of different interpretations for the size-dependent yield stress on FCC and BCC micropillars. It also points to the importance of carefully accounting for surface effects on both the stress field and dislocation mobility in the dislocation dynamics modeling of plasticity at the microscale.

Materials and Methods

Molecular Dynamics. Molecular dynamics (MD) simulations were carried out using LAMMPS (26) and MD++ (available at http://micro.stanford.edu). The molybdenum nanopillars are modeled by the Finnis–Sinclair (FS) potential (27, 28). Dislocation self-multiplication are also observed in simulations using the modified-embedded-atom-method (MEAM) model for molybdenum and the FS potential for tantalum. The gold and aluminum nanopillars are modeled by the Foiles (29) and the Mishin (30) Embedded atom method (EAM) potentials, respectively. All nanopillars are aligned along the z = [0 0 1] direction where periodic boundary conditions are applied. MD simulations were carried out under the NσT ensemble with temperature T = 300 K and different axial stresses σ_{zz}, using the velocity Verlet integrator and a time step of Δt = 1 fs. To mimic a nucleation event, a straight dislocation with various orientations and locations is introduced in the nanopillars as the initial condition, with Burgers vector $\mathbf{b}$ = ½[1 1 1] for molybdenum and tantalum and $\mathbf{b}$ = ½[0 1 1] for gold and aluminum. The dislocation motion is observed by analyzing the trajectory of the atoms.

Dislocation Dynamics. Dislocation Dynamics (DD) simulations were performed using the ParaDiS (http://paradis.stanford.edu) program (31–34), modified to include the image stress due to the cylindrical free surface (35). Molybdenum is modeled as an isotropic medium with shear modulus μ = 123 GPa and Poisson's ratio ν = 0.305. The dislocation core radius is $r_c = b$. The dislocations are described by two continuous curves lying on $(1\bar{2}1)$ and $(\bar{2}\ 1\ 1)$ planes, as illustrated in Fig. 4*G* Each curve is parameterized by a set of interior nodes that are equally spaced in the direction (y' or y'') perpendicular to the Burgers vector and a straight segment connecting to the surface node. The mobility of the surface nodes (along y' or y'' directions) is 5.6×10^2 Pa^{-1}·s^{-1}, and is 5.6×10^4 Pa^{-1}·s^{-1} for the interior nodes (along x' direction). The magnitude of the critical stress for the self-multiplication mechanism is insensitive to the numerical values of the mobility parameters.

ACKNOWLEDGMENTS. We thank Profs. J. R. Greer and D. M. Barnett for useful discussions and Drs. D. Jang and C. Garland for sharing their recent experiments. The work is supported by National Science Foundation Career Grant CMS-0547681, and Air Force Office of Scientific Research/Young Investigator Program grant, the Army High Performance Computing Research Center at Stanford, and a Benchmark Stanford Graduate Fellowship (to C.R.W.).

1. Taylor GI (1934) Plastic deformation of crystals. *Proc R Soc London* 145:362–404.
2. Kuhlmann-Wilsdorf D, Wilsdorf HGF (1964) Dislocation movement in metals. *Science* 144:17–25.
3. Hirth, JP Lothe J (1982) *Theory of Dislocations* (Wiley).
4. Bulatov VV, Abraham FF, Kubin L, Devincre B, Yip S (1998) Connecting atomistic and mesoscale simulations of crystal plasticity. *Nature* 391:669–672.
5. Hall EO (1951) The deformation and aging of mild steel III. Discussion of results. *Proc Phys Soc London Ser B* 64:747–753.
6. Petch NJ (1953) The cleavage strength of polycrystals. *J Iron Steel Inst* 174:25–28.
7. Yip S (1998) The strongest size. *Nature* 391:532–533.
8. Brenner SS (1956) Tensile strength of whiskers. *J Appl Phys* 27:1484–1491.
9. Brenner SS (1957) Plastic deformation of copper and silver whiskers. *J Appl Phys* 28:1023–1026.
10. Uchic MD, Dimiduk DM, Florando JN, Nix WD (2004) Sample dimensions influence strength and crystal plasticity. *Science* 305:986–989.
11. Bei H, *et al.* (2007) Compressive strengths of molybdenum alloy micro-pillars prepared using a new technique. *Script Mater* 57:397–400.
12. Shan ZW, Mishra RK, Asif SAS, Warren OL, Minor AM (2008) Mechanical annealing and source-limited deformation in submicrometre-diameter Ni crystals. *Nat Mater* 7:115–119.
13. Greer JR, Nix WD (2006) Nanoscale gold pillars strengthened through dislocation starvation. *Phys Rev B Condens Matter* 73:245410.
14. Zuo L, Ngan AHW, Zheng GP (2005) Size dependence of incipient dislocation plasticity in Ni_3Al. *Phys Rev Lett* 94:1–4.
15. Ngan AHW, Zuo L, Wo PC (2006) Size dependence and stochastic nature of yield strength of micron-sized crystals: A case study on Ni_3Al. *Proc R Soc London Ser A* 462:1661–1681.
16. Parthasarathy TA, Rao SI, Dimiduk DM, Uchic MD, Trinkle DR (2007) Contribution to size effect of yield strength from the stochastics of dislocation source lengths in finite samples. *Scr Mater* 56:313–316.
17. Tang H, Schwarz KW, Espinosa HD (2008) Dislocation-source shutdown and the plastic behavior of single-crystal micropillars. *Phys Rev Lett* 100:185503.
18. Tang H, Schwarz KW, Espinosa HD (2007) Dislocation escape-related size effects in single-crystal micropillars under uniaxial compression. *Acta Mater* 55:1607–1616.
19. Senger J, Weygand D, Gumbsch P, Kraft O (2008) Discrete dislocation simulations of the plasticity of micro-pillars under unaxial loading. *Scr Mater* 58:587–590.
20. Marian J, Cai W, Bulatov VV (2004) Dynamic transitions from smooth to rough to twinning in dislocation motion. *Nat Mater* 3:158–163.
21. Kelchner CL, Plimpton SJ, Hamilton JC (1998) Dislocation nucletation and defect structure during surface indentation. *Phys Rev B Condens Matter* 58:11085–11088.
22. Cawkwell MJ, Nguyen-Manh D, Woodward C, Pettifor DG, Vitek V (2005) Origin of brittle cleavage in iridium. *Science* 309:1059–1062.
23. Christiansen J, *et al.* (2002) Atomic-scale structure of dislocations revealed by scanning tunneling microscopy and molecular dynamics. *Phys Rev Lett* 88:206106.
24. Greer JR, Weinberger CR, Cai W (2008) Comparing the strength of f.c.c. and b.c.c. sub-micrometer pillars: Compression experiments and dislocation dynamics simulations. *Mater Sci Eng A* 493:21–25.
25. Brinckmann S, Kim JY, Greer JR (2008) Fundamental differences in mechanical behavior between two types of crystals at the nanoscale. *Phys Rev Lett* 100:155502.
26. Plimpton S (1995) Fast parallel algorithms for short-range molecular dynamics. *J Comput Phys* 117:1–19.
27. Finnis MW, Sinclair JE (1984) A simple empirical n-body potential for transition metals. *Philos Mag A* 50:45–55.
28. Ackland GJ, Thetford R (1987) An improved N-body semi-empirical model for body-centred cubic transition metals. *Philos Mag A* 56:15–30.
29. Park HS, Zimmerman JA (2005) Modeling inelasticity and failure in gold nanowires. *Phys Rev B* 72:054106.
30. Mishin Y, Farkas D, Mehl MJ, Papaconstantopoulos DA (1999) Interatomic potentials for monoatomic metals from experimental data and. *ab initio calculations* Phys Rev B 59:3393–3407.
31. Cai W, *et al.* (2004) in Solid Mechanics and Its Applications, vol. 115, eds Kitagawa H, Shibutani H (Kluwer Academic Publisher, Dordrecht), pp 1.
32. Bulatov VV, *et al.* (2004) Scalable line dyanamics in ParaDiS. *IEEE/ACM SuperComputing 2004 Conference Proceedings*, pp 376–378.
33. Arsenlis A, *et al.* (2007) Enabling strain hardening simulations with dislocation dynamics. *Modell Simul Mater Sci Eng* 15:553–595.
34. Bulatov VV, Cai W (2006) *Computer Simulations of Dislocations* (Oxford Univ Press, Oxford).
35. Weinberger CR, Cai W (2007) Computing the image stress in an elastic cylinder. *J Mech Phys Solids* 55:2027–2054.